TRIDIMENSIONAL CHARACTERIZATION OF EPOXY MATRIX GLASS-FIBER REINFORCED COMPOSITES

Lorenleyn De La Hoz Alford[a]; Sidnei Paciornik[a], José Roberto Moraes d'Almeida[a]; Haimon Diniz Lopes Alves[b]; Marcos H. de PinhoMauricio[a]

[a] Dept. of Chemical and Materials Engineering, PUC-Rio, Rua Marquês de São Vicente, 225, Gávea, 22451-900 Rio de Janeiro - RJ, Brazil.

[b] University of the State of Rio de Janeiro (UERJ), Rua São Francisco Xavier, 524 - 1°andar - Sala 1006 A - Maracanã, 20550-900, Rio de Janeiro – RJ, Brazil.

https://doi.org/10.21452/bccm4.2018.05.05

ABSTRACT

Composite materials are typically heterogeneous and non-isotropic. Failure mechanisms are affected by the spatial distribution of reinforcements and the quality of the adhesion at the reinforcement-matrix interface. The traditional techniques of microscopic characterization are quite limited to study this type of material, since two-dimensional sections or projections may not fully reveal the complex three-dimensional microstructure of a composite. When seeking to understand the origin of failure mechanisms, these limitations are even more important. In this work, a three-dimensional characterization methodology was developed based on x-ray microtomography (microCT). The material evaluated was a glass fiber/epoxy matrix composite reinforced by unidirectional fibers. Test specimens were tomographed before and after flexural tests. The 3D images were analysed to visualize and quantify voids and cracks, both originated in the manufacturing process and created by mechanical loading. Evaluation of the uncertainty of the procedure was performed by tomographing more than once each sample, aligning and comparing the 3D images. The analysis allowed to quantify the increase in defect volume after material failure.

Keywords
Fiber reinforced composites; failure mechanisms; microtomography; 3D visualization.

1. INTRODUCTION

Composite materials are generally formed by a continuous matrix phase and a discontinuous reinforcement phase. Traditionally, the characterization of these materials is performed by microscopy techniques, generating two-dimensional information of the material structure [1]. However, the microstructure and defects in composites are fundamentally three-dimensional. Thus, it is important to have techniques that allow this kind of analysis.

X-ray Microtomography (microCT) serves this purpose. This is a technique that offers poorer resolution than optical microscopy (OM) and scanning electron microscopy (SEM), but it is widely used in the characterization of the internal morphology of materials, creating

three-dimensional representations. MicroCT is non-destructive and does not require a previous step of sample preparation, as is the case with microscopy. MicroCT can be used in materials that have a sufficiently large density difference between their constituents or in the atomic composition in order to generate x-ray absorption contrast [2,3].

There are several results that demonstrate the feasibility of using microCT in the evaluation of the internal geometry of materials, and in the study of cracks and defects, including delamination and microcracks [4-6]. These results show that microCT images allow the visualization of defects and the analysis of the morphological characteristics of the samples, especially in the study of complex structures.

In this work, glass-fiber reinforced epoxy matrix composites were evaluated before and after bending tests by microCT. The presence of defects was visualized and quantified. A calibration procedure allowed to estimate the uncertainty of these measurements.

2. MATERIALS AND METHODS

2.1. Samples

The samples were manufactured by vacuum bagging of prepregs laminas. The epoxy matrix used was formulated by mixing the appropriated amounts of epoxy monomer, based on diglycidyl ether of bisphenol A (DGEBA), and triethylenetetramine (TETA) hardener. E-glass fibers were used as reinforcement, with a nominal volume fraction of 50%.

The analysis of cracks and defects was performed in two samples, having different geometric characteristics. Figure 1 shows the two specimens used (CP1 and CP2). CP2 has a notch, reducing its width from 12.7mm to 7mm in its central region (Figure 1b). The idea was to create a region of stress concentration to evaluate its impact on the formation/propagation of defects. Both specimens were cut in the dimensions shown in Figure 1 to allow higher spatial resolution during the analysis, which is inversely proportional to the sample thickness.

2.2. Flexural Tests

The specimens were submitted to a three-point flexural test according to ASTM D 790-10. The tests were performed in the AME-2kN equipment with a capacity of 2kN.

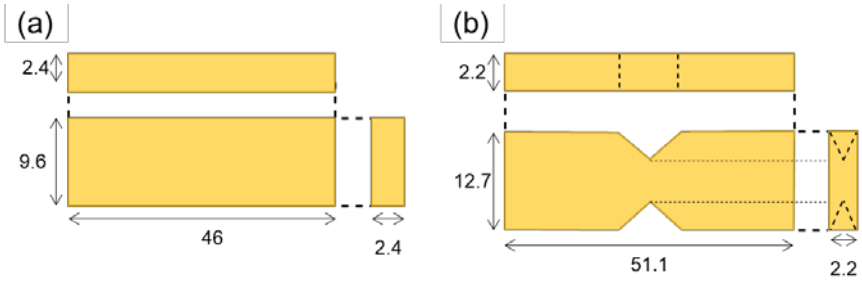

Figure 1: Schematic drawing of the specimens. (a) CP1. (b) CP2. Dimensions in mm.

2.3. MicroCT

MicroCT scans were obtained with the Zeiss Xradia 510 Versa microtomograph. This equipment combines the simple geometric magnification, dependent on source-sample-detector distances, to optical magnification obtained with an optical microscope. Each optical lens is fitted with a scintillator that converts X-rays to light.

For this analysis a resolution around 13.75 μm given by the 0.4X lens was used, allowing a complete scan of the sample in a reasonable time. In order to minimize the total time of analysis, reconstructions were tested with 800, 1600 and 3201 projections, and the intermediate value of 1600 projections was chosen. The exposure time was 0.5s, leading to a total scan time of approximately two hours. Then the layers were reconstructed with the XMReconstructor V Cone Beam-11 software.

For a better understanding of the experimental methodology, it is necessary to understand the sequence of evaluation of the uncertainty of the procedure. As defects previously present in the sample and those created by the mechanical test appear in low fraction, uncertainties caused by the conditions of acquisition and/or processing of the images could lead to non-representative results. Thus, not only the operating conditions of the CT scanner were kept constant (x-ray energy, source-sample-detector geometry, lens, exposure time, number of projections, spatial resolution), but variations in the images caused by acquisition of the images were also evaluated, without influence of the flexure tests.

The methodology was divided into 2 stages as summarized in Table 1:

1) In the first step, the sensitivity of the procedure was determined by tomographing CP1 3 times before the flexure test. The first two scans were performed in sequence, without removing the sample from the scanner. The specimen was then removed and replaced in the tomograph, and a third scan was performed. The 3 images were processed and analyzed, as described below, and the volumetric fraction of defects quantified. Any variations in this step would only be caused by uncertainties in the acquisition of the images and served as a margin of error for the results obtained in the second step.
2) In the second step, the samples were submitted to two bending tests and were scanned after each one. In the first test, the samples were tested within the elastic regime, in the assumption that the mechanical stress would not cause damages. In the second test, the samples were taken to rupture.

Table 1: Image capture steps.

Stage	Sequence	Code
1	Tomography and initial reconstruction.	I1
	Tomography without removing the sample from the tomograph.	I2
	Tomography after removing and repositioning the sample.	Ret
2	Tomography of the test material 1 time.	E1
	Tomography of the test material 2 times.	E2

2.4. Image Processing and Analysis

Once the reconstructed images were obtained, an image processing sequence was performed. This stage is usually constituted by preprocessing steps for noise reduction, segmentation for object discrimination and post-processing for filtering objects and eliminating artifacts [7]. At the end, 3D visualization and orthogonal planes of the specimens are generated. For this analysis, 3D software Dragonfly v3.5 (Object Research Systems, Canada) was used.

2.4.1. Image Registration

To monitor the impact of the mechanical stress on generation of defects, it is important to evaluate equivalent regions in the sample, before and after the bending tests. For this, a 3D alignment between the tomographic images obtained before and after the test was performed with the DataViewer program (Bruker Inc., UK).

This alignment was only possible because, even after the test, the external dimensions of the sample showed nearly no change. In fact, the alignment did not seek to correct for size and/or shape distortions generated by the mechanical test. The objective was only to correct the x-y-z displacement caused by the removal of the sample from the tomograph. Figure 2 shows two views of CP1 images I1 and E2 before and after alignment.

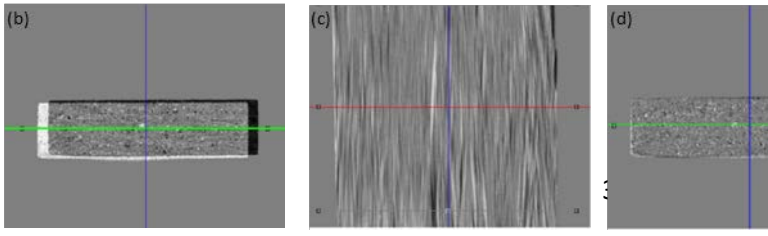

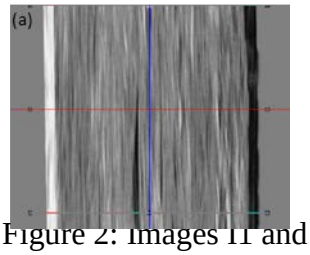

Figure 2: Images I1 and E2 of CP1 before (a, b) and after (c, d) of the 3D registration. The light and dark edges indicate the initial misalignment, corrected after the procedure.

2.4.2. Segmentation of defects and cracks

Defects and cracks appeared as darker regions within the composite matrix. The direct segmentation of these regions by tonal range was not viable, since regions external to the sample showed similar x-ray absorption and tone. Thus, the procedure involved segmenting the solid matrix, filling in the defects and subtracting, generating an image only of the defects.

The defects were filled in two stages. First, a 3D morphological closing operation with a neighborhood of 13 pixels was used to close the defects that touched the edges of the sample. Then, a hole-filling operator was applied along the x, y and z directions, successively [7,8].

The tonal threshold to segment the matrix was chosen from the 2D projections in the 3 orthogonal directions and from the 3D image. The critical point was to select the matrix without including regions corresponding to defects. To avoid introducing uncertainty, the tonal range used was kept constant for all CT scans (I1, I2, Ret, E1, E2).

Then, the matrix volumes (v_M), filled matrix (v_{MP}), which corresponds to the total volume of the specimen, and the defects $v_D = v_{MP} - v_M$, were measured. From these values, the volume fraction of defects $\% V_D = v_D / v_{MP}$ was obtained.

3. RESULTS AND DISCUSSION

3.1. Flexural test

Analysis of the stress-strain behavior during the flexure test allowed the samples to be kept within the elastic limit in the first test and to bring them to rupture in the second test. Figure 3 shows the stress-strain curves for the second test of both samples. Note that CP2 has a higher flexural strength than CP1.

As both specimens were cut from the same composite plate, the differences in the flexural test could in principle be associated with the presence of the notch in CP2. However, this should contribute to reduce flexural strength and not to increase it, as shown in Figure 3. The explanation is probably associated with the defect concentration, as explained below.

3.2. Image analysis and observation of defects and cracks

Figures 4 and 5 show images of the two samples, after the flexure test. Defects appear as dark regions against the gray background of the material.

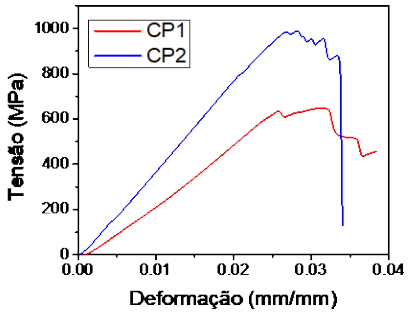

Figure 3: Comparison of stress-strain curves after the second mechanical test (E2, Table 1).

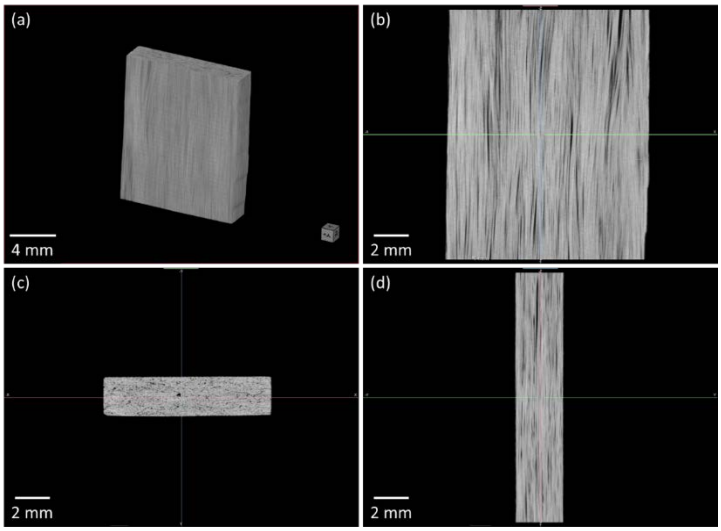

Figure 4: MicroCT image (CP1, condition E2). (a) 3D view; and planes (b) xz; (c) xy; (d) yz.

Figure 6 shows the results of defect segmentation for CP1, condition E2. The defects appear colored against the gray background formed by the material. In the 3D image, part of the sample was made transparent to show only the defects. It is worth mentioning that the 3D visualization gives the impression that the concentration of defects is much greater than in the 2D projections. This is a typical effect and depends heavily on the orientation in which the 3D image is presented. This visual effect will be criticized in the light of the quantitative analysis of defects, as described below.

Table 2 presents the volume fraction of defects (V_D) of CP1 at conditions I1, I2 and Ret (before the mechanical test), E1 (after the test at the elastic region), and E2 (after test to failure). The percentage changes, $\Delta(\%)$, with respect to the initial value, I1, are also presented.

The values for I1 and I2 are identical, indicating the stability of the image acquisition process. The values are also almost equal to Ret, indicating that errors caused by mechanical instabilities are small, ≈1% of the initial value. The value for E1 indicates a small increase of ≈6% in the defect fraction when the sample is tested within the elastic region. Finally, when the sample is taken to failure, the defect fraction increases almost 80% but does not reach 15%. This is not such a large value, which should be contrasted with the impression of high defect concentration brought by Figure 6a.

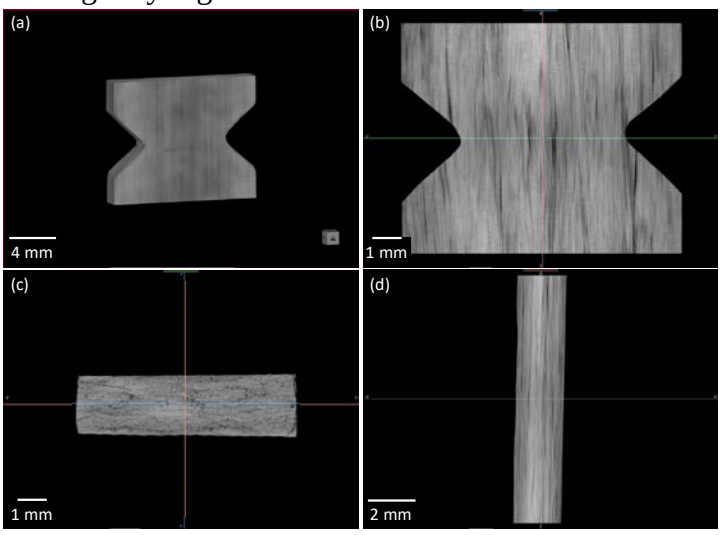

Figura 5: MicroCT image (CP2, condition E2). (a) 3D view; and planes (b) xz; (c) xy; (d) yz.

Table 2: Volumetric Defect Fraction

	CP1		CP2	
Tomographic Stage	V_D (%)	Δ (%)	V_D (%)	Δ (%)
I1	7.8	–	1.0	–
I2	7.8	0		
Ret	7.9	1.3		
E1	8.3	6.4		
E2	14.0	79.5	3.0	200

Figure 7 presents the defect analysis for CP2 in the E2 condition. In this case, the defect fraction is apparently smaller, which is confirmed by the quantitative analysis. The values for the defect fraction of CP2 are presented in Table 2 for the original condition (I1) and after the test until the rupture (E2). The initial volume fraction is much lower than that of CP1, but grows 200% after the test. Its maximum value reaches 3%, about 5 times less than in CP1. This large difference may explain the results of the bending test. Despite the notch, CP2 has a higher flexural strength, probably because it contains less defects than CP1.

Despite the smaller fraction of defects in CP2, a comparative visual analysis between states I1 and E2 brings relevant information. Figure 8 shows the presence of preexisting defects in the sample (pink rectangles) and defects generated during the flexure test (red rectangles).

To make the comparison more representative, the images of conditions I1 and E2 were aligned (section 2.4.1), the defects were segmented and overlapped (Figure 9). The appearance of cracks during the test, especially in the notch region, is evident. It can be observed that the upper right crack does not change after the test, but several new cracks appear. In polymer composites there are several failure modes, which can occur in the fiber, matrix or fiber-matrix interface. However, with the resolution employed in this work it was not possible to identify the main failure mode for this composite [11].

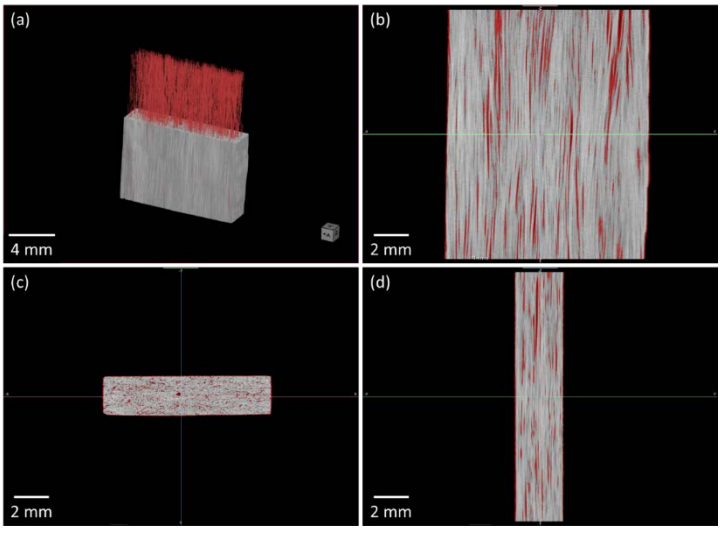

Figure 6: Defect detection - CP1 (condition E2). (a) 3D view; and planes (b) xz; (c) xy; (d) yz.

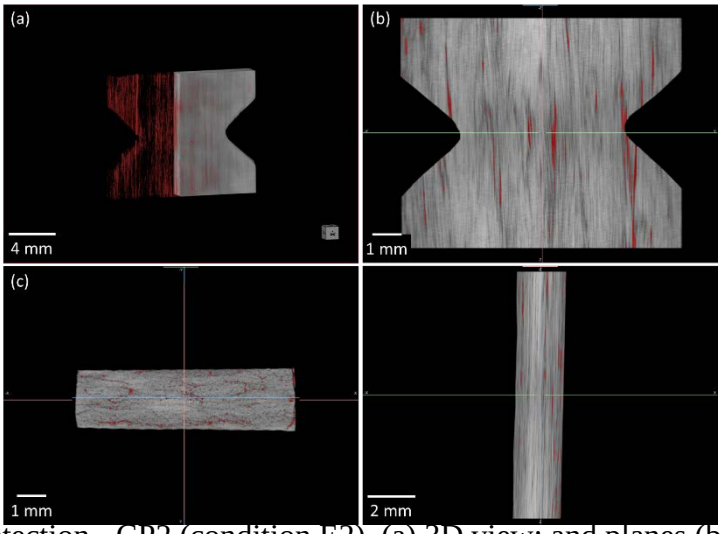

Figure 7: Defect detection - CP2 (condition E2). (a) 3D view; and planes (b) xz; (c) xy; (d) yz.

4. CONCLUSIONS

This work presented a methodology for the characterization of glass-fiber reinforced epoxy matrix composites from the 3D image analysis of microCT images.

From the qualitative point of view, the methodology allowed 3D visualization of defects formed as a function of the application of mechanical stress in the material. It was possible to compare the same specimen before and after a bending test, discriminating pre-existing cracking defects caused by mechanical stress.

The quantitative analysis, preceded by a sensitivity evaluation step, allowed to directly measuring the volumetric fraction of defects as a function of the applied stress level. As expected, the defect fraction remained approximately constant in the elastic regime and increased substantially upon reaching the material rupture stress.

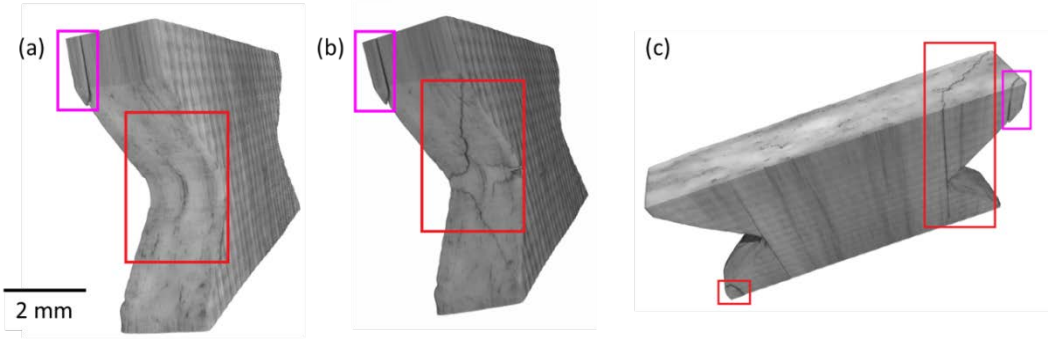

Figure 8: 3D visualization of defects and cracks in CP2. (a) Before the test (I1); b) and c) After the test (E2). Pre-existing crack (pink). Cracks generated by the test (red).

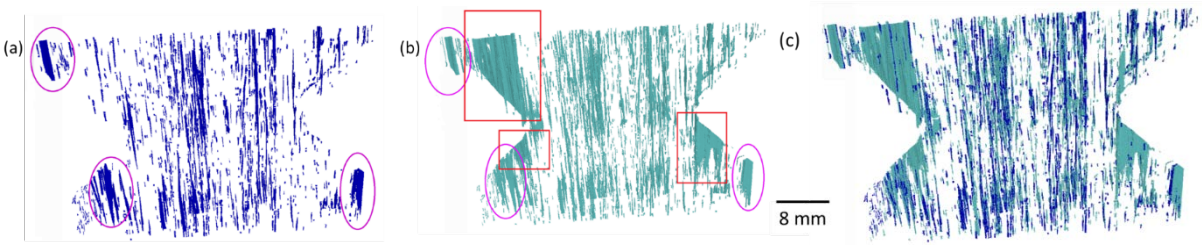

Figure 9: Comparative visualization of defects in CP2. (a) Condition I1; (b) Condition E2. Pre-existing defects (pink ellipses) and generated during the test (red rectangles).

(c) Overlap of (a) and (b).

6. REFERENCES

[1] Evolution in the Characterization of Composite Materials through Digital Microscopy. Materials Science Research Journal 1(3/4) (2008) 331-383.

[2] ALVES H, LIMA I, LOPES RT. Methodology for attainment of density and effective atomic number through dual energy technique using microtomographic images. Applied Radiation and Isotopes **89**, 6-12, 2014.

[3] MEES, F; SWNNER, R.; VAN GEET, M.; AND JACOBS (EDS), P. Applications of x-ray computed tomography in the geosciences. Geological Society, Special Publications 215, 1-6, 2003.

[4] BUFFIÈREÁ J.-Y; MAIRE E.; CLOETENSB P.; LORMANDA G. AND FOUGÈRESÁ R. Characterization of internal damage in a MMCp using x-ray synchrotron phase contrast microtomography. Acta Materialia, **47**, 5, 1613-1625, 1999.

[5] SHILLING, P.; KAREDLA, B.; TATIPARTHI, A.; VERGES, M. & HERRINGTON, P. X-ray computed microtomography of internal damage in fiber reinforced polymer matrix composites. Composites science and technology, **65**, 14, 2071-2078, 2005.

[6] FIDAN, S.; SINMAZÇELIK, T.; AVCU, E. Internal damage investigation of the impacted glass/glass + aramid fiber reinforced composites by microcomputerized tomography. NDT&E International, **51**, 1-7, 2012.

[7] PACIORNIK, S. and MAURÍCIO, M H P. Digital Imaging, in: *ASM Handbook Volume 9: Metallography and Microstructures* (ed: G F Vander-Voort), pp 368-402 (ASM International: Materials Park), 2004

[8] SERRA, J. Image Analysis and Mathematical Morphology, Academic Press: London, 1982.

[9] AMBUR D. R.; STARNES J. H.; PRASAD, C. B. Low-speed Impact Damage-Initiation Characteristics of Selected Laminated Composite Plates. AIAA Journal, **33**, 10, 1919-1925, 1995.